

Anomalous Resistivity and Electron Heating by Lower Hybrid Drift Waves during Magnetic Reconnection with a Guide Field

Jongsoo Yoo^{1,*}, Jonathan Ng², Hantao Ji^{1,3}, Sayak Bose¹, Aaron Goodman,⁴ Andrew Alt,³
Li-Jen Chen⁵, Peiyun Shi¹ and Masaaki Yamada¹


¹*Princeton Plasma Physics Laboratory, Princeton, New Jersey 08542, USA*

²*Department of Astronomy, University of Maryland, College Park, Maryland 20742, USA*

³*Department of Astrophysical Sciences, Princeton University, New Jersey 08544, USA*

⁴*Department of Mechanical and Aerospace Engineering, Princeton University, New Jersey 08544, USA*

⁵*NASA Goddard Space Flight Center, Greenbelt, Maryland 20771, USA*

 (Received 10 May 2023; revised 29 December 2023; accepted 7 February 2024; published 4 April 2024)

The lower hybrid drift wave (LHDW) has been a candidate for anomalous resistivity and electron heating inside the electron diffusion region of magnetic reconnection. In a laboratory reconnection layer with a finite guide field, quasielectrostatic LHDW (ES-LHDW) propagating along the direction nearly perpendicular to the local magnetic field is excited in the electron diffusion region. ES-LHDW generates large density fluctuations (δn_e , about 25% of the mean density) that are correlated with fluctuations in the out-of-plane electric field (δE_Y , about twice larger than the mean reconnection electric field). With a small phase difference ($\sim 30^\circ$) between two fluctuating quantities, the anomalous resistivity associated with the observed ES-LHDW is twice larger than the classical resistivity and accounts for 20% of the mean reconnection electric field. After we verify the linear relationship between δn_e and δE_Y , anomalous electron heating by LHDW is estimated by a quasilinear analysis. The estimated electron heating is about 2.6 ± 0.3 MW/m³, which exceeds the classical Ohmic heating of about 2.0 ± 0.2 MW/m³. This LHDW-driven heating is consistent with the observed trend of higher electron temperatures when the wave amplitude is larger. Presented results provide the first direct estimate of anomalous resistivity and electron heating power by LHDW, which demonstrates the importance of wave-particle interactions in magnetic reconnection.

DOI: [10.1103/PhysRevLett.132.145101](https://doi.org/10.1103/PhysRevLett.132.145101)

Magnetic reconnection is a fundamental physics process through which energy in the magnetic field is rapidly converted into plasma energy via rearrangement of magnetic topology [1,2]. Magnetic reconnection has been considered to play a key role in solar flares, in Earth's magnetosphere, and during rapid energy release in astrophysics such as accretion onto black holes. It has been an outstanding challenge in identifying the responsible kinetic mechanisms for efficient dissipation to allow fast reconnection in nearly collisionless plasmas, where the classical resistivity is negligibly unimportant. Nongyrotropic pressure tensor has been confirmed as a two-dimensional (2D) kinetic mechanism [3–5] to break and reconnect field lines. However, the kinetic anomalous dissipation mechanisms generally operating in 3D still remain unclear despite the long research history [2] within or nearby diffusion regions where abundant free energy exists for waves and instabilities [6,7]. Candidate plasma waves and instabilities [8] include whistler waves [9,10], Buneman instabilities [11–13], ion acoustic waves [14–17], drift kink [18], or kinetic Kelvin-Helmholtz instabilities [19].

These waves and instabilities may impact on reconnection and electron dynamics by producing fluctuations in

fields and plasma parameters [13,20,21]. The effects of fluctuations can be quantified by examining an average of second-order terms. For example, the anomalous drag (resistivity) term is defined as [22]

$$D = -\frac{\langle \delta n_e \delta E_Y \rangle}{\langle n_e \rangle}, \quad (1)$$

where $\langle \dots \rangle$ denotes a temporal average of a physical parameter, n_e is the electron density, δn_e is the electron density fluctuation, and δE_Y is the electric field fluctuation along the direction normal to the reconnection plane (Y). This second order term becomes significant when both fluctuating quantities are comparable to or larger than their mean values and there are positive correlations between δn_e and δE_Y . In this case, the momentum transfer between electrons and ions are enhanced by the amount of D .

The lower hybrid drift wave (LHDW), driven by cross-field gradient [23] or cross-field relative drift between ions and electrons [24,25], has been a candidate for anomalous resistivity as it interacts both with ions and electrons, potentially enhancing the momentum exchange between two species [26–30]. With a similar electron temperature

and perpendicular current density, the electron beta ($\beta_e = 2\mu_0 n_e T_e / B^2$; μ_0 is the vacuum magnetic permeability, T_e is the electron temperature, and B is the strength of the magnetic field) controls the type of LHDW [31]. With a relatively small β_e , LHDW is quasiaelectrostatic (ES-LHDW) [32,33], while it becomes electromagnetic (EM-LHDW) [34,35], when β_e is larger.

EM-LHDW, propagating obliquely to the magnetic field, is featured with large fluctuations in the magnetic field with frequencies below the local lower hybrid frequency ($f_{\text{LH}} = \sqrt{f_{\text{ce}} f_{\text{ci}}}$; f_{ce} and f_{ci} are the electron and ion cyclotron frequency, respectively). It has been frequently observed in the electron diffusion regions (EDR) [27,29,30,34–37]. Despite early signatures of its importance in generating anomalous dissipation, however, EM-LHDW does not seem to play an important role in fast reconnection [29,38], at least within the parameters that it has been studied.

In contrast, ES-LHDW, propagating nearly perpendicular to the magnetic field, is featured with large fluctuations in the electric field usually with frequencies below f_{LH} [31–33,39–44]. ES-LHDW is frequently observed near separatrix regions on the low-density side [32,44,45]. Without a guide field, however, ES-LHDW becomes EM-LHDW in the EDR due to the high local beta [31,32,46], such that its effects on anomalous resistivity is limited. Recently, observations by the magnetospheric multiscale (MMS) spacecraft have shown the ES-LHDW with a large amplitude when local β_e is small during guide field reconnection either inside the current sheet [31,43] or the downstream region [47], but without anomalous dissipation due to the ideal electron-magnetohydrodynamic nature of the observed waves [21].

In this Letter, we report the first direct laboratory evidence of anomalous resistivity by ES-LHDW during magnetic reconnection with a guide field. The experiments were performed on the magnetic reconnection experiment (MRX) [48], where n_e and T_e as well as δn_e and δE_Y [33] are directly measured and the fluctuation quantities are confirmed to follow the predicted linear relationship based on dispersion relation of ES-LHDW. The experimentally determined anomalous resistivity is found to be more important for the first time than classical resistivity in any laboratory reconnection experiments. In addition, anomalous heating by LHDW from quasilinear analysis [49] exceeds the classical Ohmic heating.

MRX has a cylindrical vacuum vessel with 1.5 m of the diameter and about 2 m of height. Figure 1(a) shows a cross section of MRX in the RZ plane. Here we employ a local Cartesian coordinate system with R for the radial direction, Z for the axial direction, and Y for the toroidal direction. The gray circles indicate doughnut-shape flux cores inside which two independent sets of coils drive reconnection and create plasma [48]. The main diagnostic is a 2D magnetic probe array with about 250 miniature pickup coils [35,50].

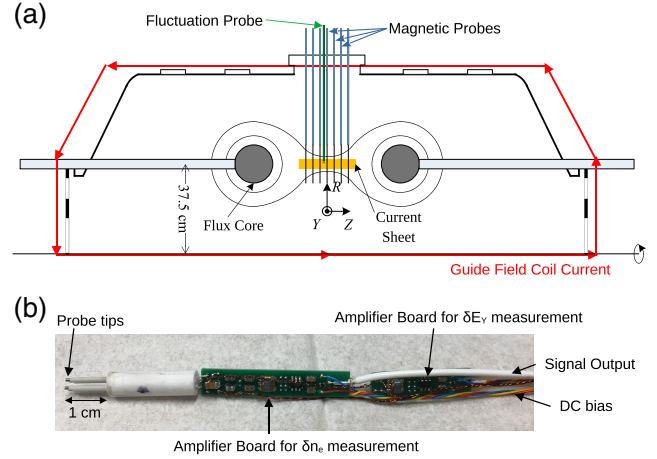


FIG. 1. (a) Cross section of the cylindrical MRX vessel with the local RYZ coordinate system. Flux cores contains two independent sets of internal coils. In addition, GF coils generate a relatively uniform out-of-plane magnetic field. We insert magnetic probes and a special fluctuation probe to measure the field geometry and fluctuations in the reconnection electric field and density. (b) Photo of the fluctuation probe with four tips and two miniature amplifier boards. Two floating tips are connected to the board for δE_Y , while two biased tips are connected to that for δn_e .

Assuming the toroidal symmetry, this probe array can provide 2D profiles of the magnetic field (\mathbf{B}), the current density (\mathbf{J}), and the reconnection electric field ($E_{\text{rec}} = -E_Y$). The Lundquist number of the plasma is about 300 and the system size normalized to the ion sound radius is about 20, which means that the plasma is in the single X line, collisionless regime [2,51]. The plasma in the current sheet is weakly collisional: collisional effects are finite but unimportant.

In addition, an electrostatic probe is inserted radially with the tip location of $(R, Z) = (37.5, -1.5)$ cm. As shown in Fig. 1(b), the probe has four tips with two miniature amplifier boards. Two floating tips separated by 2 mm along the Y direction provide the local floating potential. Two tips with a fixed bias voltage of 30–35 V are used to measure the ion saturation current. This typical triple Langmuir probe setup provides low-frequency measurements of n_e and T_e [52]. In addition, we also measure high-frequency fluctuations in the difference of two floating potential and the ion saturation current via the miniature amplifier boards, which can be converted to δE_Y and δn_e , respectively. Measurement errors are estimated to be around 10% mostly due to typical uncertainties in the electrostatic probe measurement. Detailed information of this probe can be found in the reference of Hu *et al.* [33].

Interesting wave activity is consistently observed near the X line of reconnection with a moderate guide field (GF), $B_g/B_{\text{rec}} \sim 0.7$. Here B_g is absolute value of the guide field at the X line, while B_{rec} is the strength of the reconnecting field component in the upstream region. Figure 2(a) shows the profile of the out-of-plane current density (J_Y)

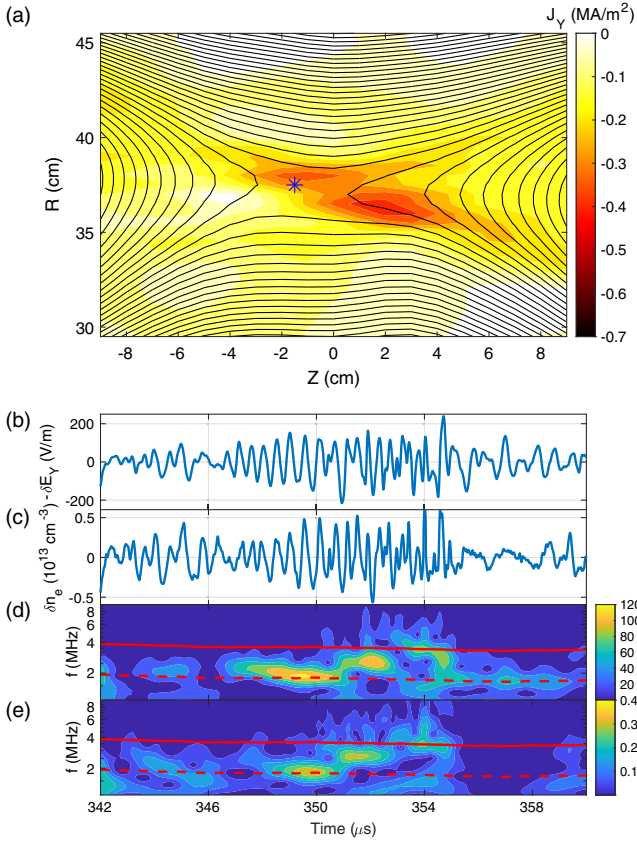


FIG. 2. Overview of MRX discharge 191 235 with a moderate guide field ($B_g/B_{\text{rec}} \sim 0.7$). (a) Profile of the out-of-plane current density (color contours) with the poloidal flux lines representing magnetic field lines at $t = 348 \mu\text{s}$. The blue asterisk indicates the location of the fluctuation probe. (b) Fluctuations in the reconnection electric field (V/m) measured by the fluctuation probe. (c) Fluctuations in the electron density (10^{13} cm^{-3}) measured by the same fluctuation probe. There is strong correlation between $-\delta E_Y$ and n_e . (d) Spectrogram of the electric field fluctuation. The red line indicates the local lower hybrid frequency, f_{LH} , while the red dashed line denotes $0.5f_{\text{LH}}$. (e) Spectrogram of the density fluctuation.

at $t = 348 \mu\text{s}$ of discharge 191 235. The black lines are the contours of the poloidal magnetic flux, representing magnetic field lines [35]. The probe (blue asterisk) is located near the X line from 342 to 366 μs , as the motion of the X line is minimal in this discharge. Important plasma and field parameters at the probe location are $T_e \sim 7.9 \text{ eV}$, $n_e \sim 2.0 \times 10^{13} \text{ cm}^{-3}$, and $B_g \sim 110 \text{ G}$, yielding the electron beta of 0.53. The current density parallel to the magnetic field is 0.27 MA/m^2 , while the perpendicular current density is 0.073 MA/m^2 . It should be also mentioned that there is density asymmetry across the current sheet with a ratio of 2–3 for all cases presented here.

We observed fluctuations in E_{rec} and n_e , as shown in Figs. 2(b) and 2(c). Two fluctuations, especially from $t = 347$ to $354 \mu\text{s}$, are well correlated and nearly in phase with each other. The amplitude of δE_Y is $\sim 150 \text{ V/m}$, which is

about twice larger than the mean reconnection electric field $\langle E_{\text{rec}} \rangle$ of about 80 V/m . The amplitude of δn_e is $\sim 0.5 \times 10^{13} \text{ cm}^{-3}$, which is about 25% of the mean density. Spectrograms of δE_Y and δn_e , shown in Figs. 2(d) and 2(e), respectively, indicate that most wave energy is below the local lower hybrid frequency (f_{LH}), denoted by the red line. This observed feature—strong electric field and density fluctuations below f_{LH} is consistent with that of ES-LHDW [31,32].

Data displayed in Figs. 2(b) and 2(c) are enough to compute the anomalous drag term D . With the measured phase difference of about 30° , $D \approx -0.5|\delta n_e||\delta E_Y|/\langle n_e \rangle \cos 30^\circ \approx 16 \text{ V/m}$, which accounts for 20% of the average reconnection electric field. This value also exceeds the contribution from the classical resistivity $\sim \eta_{\parallel} J_{\parallel} \sim 7 \text{ V/m}$. Here η_{\parallel} and J_{\parallel} are the parallel Spitzer resistivity and the parallel current density; near the electron diffusion region, the magnetic field is along the Y direction due to the sizable guide field. The rest of the reconnection electric field should be balanced by either other kinetic effects such as the nongyrotropic pressure tensor [3–5] or other anomalous effects from higher-frequency fluctuations. The additional resistivity from electron neutral collisions accounts for less than 2 V/m in this plasma.

Since our measurements of fluctuating quantities are limited to δn_e and δE_Y , we need a different approach to compute other anomalous terms. Here results from a linear theoretical model with collisional effects are used to obtain the relation among fluctuating quantities. Prior to this, however, we need to verify that the linear relationship from the model is valid in this case as the amplitude of the electric field fluctuation is large.

First, we confirm that a local theoretical model with collisional effects [49] successfully predicts that ES-LHDW is unstable near the X line in this discharge. This model calculates complex wave frequency for given k (magnitude of the wave vector \mathbf{k}) and θ (angle between \mathbf{k} and the magnetic field \mathbf{B}) in the ion rest frame. This local model does not include effects from the global shape of the current sheet, as the propagation of the wave along the density gradient direction is ignored. With the aforementioned field and plasma parameters, the dispersion relation of LHDW is obtained.

Figures 3(a) and 3(b) show the real and imaginary component of ω normalized to ω_{LH} (angular lower hybrid frequency) as a function of k and θ , respectively. The model expects that ES-LHDW is unstable near the X line with the maximum growth rate of $0.2\omega_{\text{LH}}$ at $(k\rho_e, \theta) = (0.63, 90^\circ)$, as denoted by red X marks. Here, ρ_e is the local electron gyro radius. In the lab frame, this indicates that the wave mostly propagates along the electron outflow, which is consistent with recent simulations [53]. The real frequency with the maximum growth rate is about $0.27\omega_{\text{LH}}$, which is different from observed frequency of $\sim 0.5\omega_{\text{LH}}$. This discrepancy is due to the frame difference; the results from

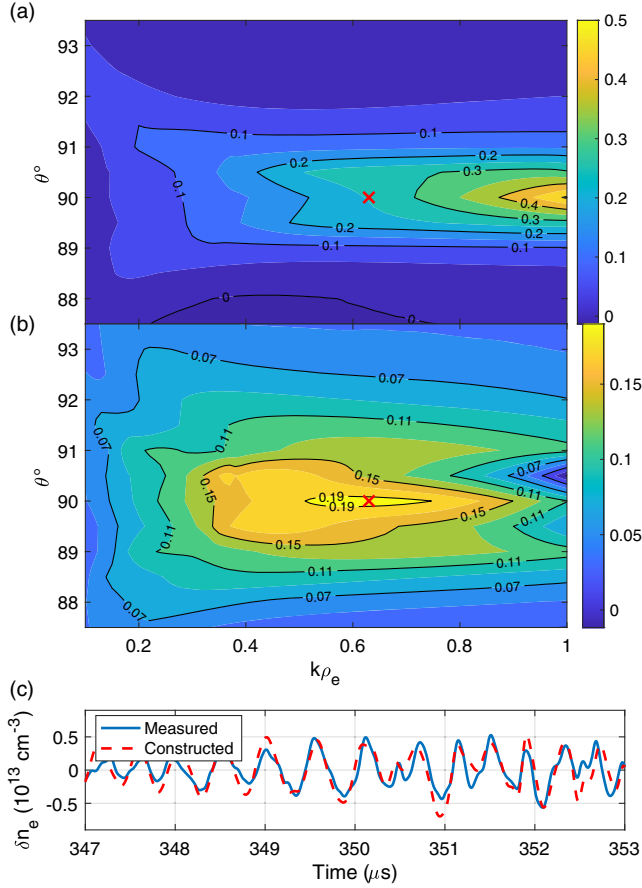


FIG. 3. (a) Real part of the angular frequency as a function of $k\rho_e$ and θ . The value is normalized to ω_{LH} . Results are from a local linear model with collisional effects [49]. The red \times mark indicates the mode with the maximum growth rate. (b) Growth rate normalized to ω_{LH} as a function of $k\rho_e$ and θ . The theoretical model expects a strong growth rate of about $0.2\omega_{LH}$ at $(k\rho_e, \theta) = (0.63, 90^\circ)$. (c) Comparison between the measured (blue solid line) and the reconstructed (red dashed line) density fluctuation. It is reconstructed with the measured δE_Y and the linear relation calculated by the collisional model. In terms of both amplitude and phase, they are in agreement.

the model is for the ion rest frame. Considering the measured ion flow of 5 km/s along the $-Z$ direction in similar discharges, the frequency of LHDW becomes $\sim 0.5\omega_{LH}$ in the lab frame, which is consistent with the measured frequency.

Finally, we verify that the linear relationship between δn_e and δE_Y from the model agrees with measurements. As shown in Fig. 3(c), the reconstructed δn_e (red dashed line) agrees well with the measured δn_e (blue line) in both the amplitude and phase. This means that the observed ES-LHDW is in the linear regime, such that other anomalous terms can be estimated with the linear relationship from the model.

The detailed process of the δn_e reconstruction from δE_Y should be mentioned. Via this linear model, all quantities such as δn_e can be expressed as a function of δE_Y with a

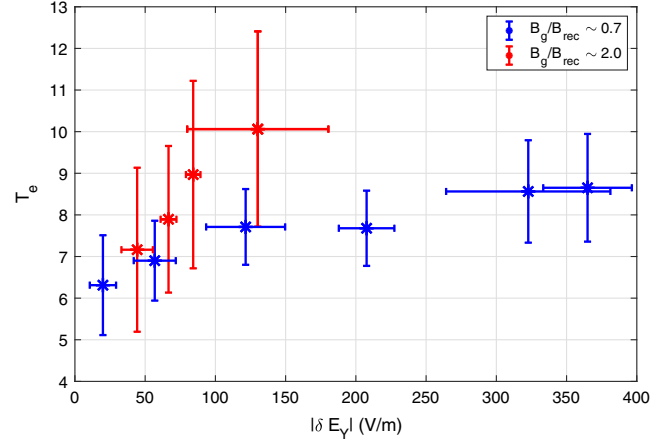


FIG. 4. Electron temperature (T_e) as a function of the amplitude ($|\delta E_Y|$) of LHDW near the X line for both moderate (blue asterisks) and high (red) GF cases. Error bars represent standard deviations of each dataset. There is a general trend that T_e is higher with larger δE_Y .

complex coefficient A ; $\delta n_e(k, \theta) = A(k, \theta)\delta E_Y(k, \theta)$. This complex coefficient, representing the linear relationship between the two fluctuating quantities, is a function of both k and θ . For strict comparison, we need to know $\delta E_Y(k, \theta)$ for all modes, which is not possible as δE_Y can only be expressed as a function of the frequency via the Fourier transform. We notice that the wave energy is mostly concentrated around $0.5f_{LH}$ and that A is a weak function of both k and θ around the maximum growth rate. Thus, it is justifiable to use the linear relation coefficient of the mode with the maximum growth rate, $A(k_{max}, \theta_{max})$ for $\delta E_Y(f)$. Then, δn_e can be reconstructed by an inverse Fourier transform of $A(k_{max}, \theta_{max})\delta E_Y(f)$.

Since this model includes all terms associated with Coulomb collisions, anomalous electron heating can also be estimated via quasilinear calculation. The anomalous electron heating term can be estimated by $\langle \delta \mathbf{J}_e \cdot \delta \mathbf{R} \rangle$, where $\delta \mathbf{J}_e$ is the first-order electron current and $\delta \mathbf{R}$ is the first-order drag force. Heating can be understood as a result of the work done by electrons when moving against the frictional force \mathbf{R} . After ignoring the negligible contribution from temperature fluctuations to $\delta \mathbf{R}$, this anomalous electron heating term is estimated to be about 2.6 MW/m^3 with $|\delta E_Y| \sim 150 \text{ V/m}$. This exceeds the classical Ohmic heating of $\eta_{\parallel} J_{\parallel}^2 + \eta_{\perp} J_{\perp}^2 \sim 2.0 \text{ MW/m}^3$.

Figure 4 demonstrates the relation between the wave amplitude and the local electron temperature in about 200 discharges. Two sets of data are presented; blue asterisks indicate data from reconnection with a moderate guide field ($B_g/B_{rec} \sim 0.7$, including discharge 191 235), while red asterisks are data points from reconnection with a high guide field ($B_g/B_{rec} \sim 2.0$). In both cases, there is a trend that T_e is higher with larger $|\delta E_Y|$. In all cases, the location of the probe is within 2 cm ($\sim 10d_e$) of the X point and T_e

and $|\delta E_Y|$ are averaged over 1.6 μs . Each data point represents the average of about 25 discharges with a similar wave amplitude and β_e ; for the moderate GF case, $0.5 < \beta_e < 0.7$, while $0.03 < \beta_e < 0.15$ for the high GF case. There is also no strong variance in the baseline electron temperature in the upstream region and reconnection electric field. Error bars are based on the standard deviation of each dataset.

It is worth noting that expected electron heating is more significant in the high GF case, while the amplitude of δE_Y is stronger in the moderate GF case. Since there is not much difference in the plasma parameters between two cases, this difference in heating could be related to better local confinement by the large GF [54]; with a larger GF, the dominant parallel electron heat flux in the reconnection plane may be significantly reduced as the magnetic field direction is mostly along the out-of-plane (symmetric) direction. Moreover, the perpendicular heat flux in the reconnection plane is relatively much smaller than the parallel heat flux. As a result, the heat flux within the reconnection plane decreases with a strong guide field, which may produce higher local electron temperature. Information on the local electron heat flux is required to verify this effect, which can be obtained by either an estimate based on electron density and temperature profiles or a direct measurement from the electron distribution function.

Another interesting observation is that when the amplitude of LHDW in the high GF case exceeds about 200 V/m, the LHDW spectrum becomes broadband (turbulent), limiting the fluctuation amplitude. For the moderate GF case, on the other hand, the LHDW spectrum does not become turbulent even when the amplitude is larger than 400 V/m. This nonlinear behavior of LHDW and its strong dependence on GF are a potential future research topic.

A future research is related to electron heating by LHDW via Landau damping [55]. To estimate this, we need to know the amplitude of each mode [$\delta E_Y(k, \theta)$], which is not available. Moreover, unlike the n_e reconstruction, the mode with the maximum growth rate cannot represent the Landau damping, because $k_{\parallel} = 0$ for the mode; electrons are resonant with LHDW along the parallel direction, so that a finite parallel wave number (k_{\parallel}) is required to meet the resonance condition of $v_e = \omega/k_{\parallel}$. As result, it is very difficult to estimate collisionless heating with the limited laboratory data. Thus, we plan to address this subtle but interesting topic via simulations and data of electron distribution functions from MMS.

In summary, we present the first quantitative laboratory results showing that ES-LHDW directly contributes to both momentum exchange between electrons and ions and electron heating in the electron diffusion region. A typical example shows that both anomalous resistivity and heating terms exceed those of classical terms. The linear relation between δE_Y and δn_e from the collisional theory agrees

with measurements. The theory tells us that the small phase difference between δE_Y and δn_e is mostly due to effects from the Lorentz force term. The physics behind the anomalous resistivity will be found in the Supplemental Material [56]. We also plan to quantify the effects of LHDWs on electron dynamics with a different guide field, including the electromagnetic LHDW that were observed before [27,30,34,36,37,44].

The data that support the findings of this study are openly available in the Princeton Data Commons [57].

This work was supported by the DOE Contract No. DEAC0209CH11466, NASA Grants No. NNH20ZDA001N, No. 80HQTR21T0060, No. 80NSSC21K1462, No. 80NSSC21K1795, and No. 80HQTR21T0105, and the NASA MMS Project.

*jyoo@pppl.gov

- [1] M. Yamada, R. Kulsrud, and H. Ji, *Rev. Mod. Phys.* **82**, 603 (2010).
- [2] H. Ji, W. Daughton, J. Jara-Almonte, A. Le, A. Stanier, and J. Yoo, *Nat. Rev. Phys.* **4**, 263 (2022).
- [3] M. Hesse, K. Schindler, J. Birn, and M. Kuznetsova, *Phys. Plasmas* **6**, 1781 (1999).
- [4] J. L. Burch *et al.*, *Science* **352**, aaf2939 (2016).
- [5] R. B. Torbert *et al.*, *Science* **362**, 1391 (2018).
- [6] K. Fujimoto, I. Shinohara, and H. Kojima, *Space Sci. Rev.* **160**, 123 (2011).
- [7] Y. V. Khotyaintsev, D. B. Graham, C. Norgren, and A. Vaivads, *Front. Astron. Space Sci.* **6**, 70 (2019)..
- [8] K. Papadopoulos, *Rev. Geophys. Space Phys.* **15**, 113 (1977).
- [9] C. Kennel and H. Petschek, *J. Geophys. Res.* **71**, 1 (1966).
- [10] M. V. Goldman, D. L. Newman, G. Lapenta, L. Andersson, J. T. Gosling, S. Eriksson, S. Markidis, J. P. Eastwood, and R. Ergun, *Phys. Rev. Lett.* **112**, 145002 (2014).
- [11] O. Buneman, *Phys. Rev. Lett.* **1**, 8 (1958).
- [12] J. Drake, M. Swisdak, C. Cattell, M. Shay, B. Rogers, and A. Zeiler, *Science* **299**, 873 (2003).
- [13] H. Che, J. F. Drake, and M. Swisdak, *Nature (London)* **474**, 184 (2011).
- [14] B. Coppi and A. B. Friedland, *Astrophys. J.* **169**, 379 (1971).
- [15] D. F. Smith and E. R. Priest, *Astrophys. J.* **176**, 487 (1972).
- [16] F. Coroniti and A. Evitar, *Astrophys. J. Suppl. Ser.* **33**, 189 (1977).
- [17] R. Z. Sagdeev, *Rev. Mod. Phys.* **51**, 1 (1979).
- [18] W. Daughton, *J. Geophys. Res.* **104**, 28701 (1999).
- [19] T. K. M. Nakamura, H. Hasegawa, W. Daughton, S. Eriksson, W. Y. Li, and R. Nakamura, *Nat. Commun.* **8**, 1582 (2017).
- [20] H. Che, *Phys. Plasmas* **24**, 082115 (2017).
- [21] D. B. Graham, Y. V. Khotyaintsev, A. Vaivads, M. Andre, C. Norgren, J. Drake, P.-A. Linqvist, O. Le Contel, R. Ergun, D. Gershman, B. Giles, C. Russell, W. Magnes, J. Burch,

- R. Torbert, K.-J. Hwang, and K. Dokgo, *Nat. Commun.* **13**, 2954 (2022).
- [22] F. S. Mozer, M. Wilber, and J. F. Drake, *Phys. Plasmas* **18**, 102902 (2011).
- [23] N. Krall and P. Liewer, *Phys. Rev. A* **4**, 2094 (1971).
- [24] J. McBride, E. Ott, J. Boris, and J. Orens, *Phys. Fluids* **15**, 2367 (1972).
- [25] R. C. Davidson and N. T. Gladd, *Phys. Fluids* **18**, 1327 (1975).
- [26] I. Silin, J. Büchner, and A. Vaivads, *Phys. Plasmas* **12**, 062902 (2005).
- [27] R. Kulsrud, H. Ji, W. Fox, and M. Yamada, *Phys. Plasmas* **12**, 082301 (2005).
- [28] P. H. Yoon and A. T. Y. Lui, *J. Geophys. Res.* **112**, A06207 (2007).
- [29] V. Roytershteyn, W. Daughton, H. Karimabadi, and F. S. Mozer, *Phys. Rev. Lett.* **108**, 185001 (2012).
- [30] V. Roytershteyn, S. Dorfman, W. Daughton, H. Ji, M. Yamada, and H. Karimabadi, *Phys. Plasmas* **20**, 061212 (2013).
- [31] J. Yoo, J.-Y. Ji, M. V. Ambat, S. Wang, H. Ji, J. Lo, B. Li, Y. Ren, J. Jara-Almonte, L.-J. Chen, W. Fox, M. Yamada, A. Alt, and A. Goodman, *Geophys. Res. Lett.* **47**, e2020GL087192 (2020).
- [32] T. A. Carter, H. Ji, F. Trintchouk, M. Yamada, and R. M. Kulsrud, *Phys. Rev. Lett.* **88**, 015001 (2001).
- [33] Y. Hu, J. Yoo, H. Ji, A. Goodman, and X. Wu, *Rev. Sci. Instrum.* **92**, 033534 (2021).
- [34] H. Ji, S. Terry, M. Yamada, R. Kulsrud, A. Kuritsyn, and Y. Ren, *Phys. Rev. Lett.* **92**, 115001 (2004).
- [35] J. Yoo, M. Yamada, H. Ji, J. Jara-Almonte, C. E. Myers, and L.-J. Chen, *Phys. Rev. Lett.* **113**, 095002 (2014).
- [36] H. Ji, R. Kulsrud, W. Fox, and M. Yamada, *J. Geophys. Res.* **110**, A08212 (2005).
- [37] A. von Stechow, W. Fox, J. Jara-Almonte, J. Yoo, H. Ji, and M. Yamada, *Phys. Plasmas* **25**, 052120 (2018).
- [38] V. Roytershteyn, S. Dorfman, W. Daughton, H. Ji, M. Yamada, and H. Karimabadi, *Phys. Plasmas* **20**, 061212 (2013).
- [39] C. Norgren, A. Vaivads, Y. V. Khotyaintsev, and M. André, *Phys. Rev. Lett.* **109**, 055001 (2012).
- [40] D. B. Graham *et al.*, *J. Geophys. Res.* **122**, 517 (2017).
- [41] D. B. Graham, Y. V. Khotyaintsev, C. Norgren, A. Vaivads, M. André, J. F. Drake, J. Egedal, M. Zhou, O. Le Contel, J. M. Webster, B. Lavraud, I. Kacem, V. Génot, C. Jacquy, A. C. Rager, D. J. Gershman, J. L. Burch, and R. E. Ergun, *J. Geophys. Res.* **124**, 8727 (2019).
- [42] L.-J. Chen, S. Wang, M. Hesse, R. E. Ergun, T. Moore, B. Giles, N. Bessho, C. Russell, J. Burch, R. B. Torbert, K. J. Genestreti, W. Paterson, C. Pollock, B. Lavraud, O. Le Contel, R. Strangeway, Y. V. Khotyaintsev, and P.-A. Lindqvist, *Geophys. Res. Lett.* **46**, 6230 (2019).
- [43] L.-J. Chen *et al.*, *Phys. Rev. Lett.* **125**, 025103 (2020).
- [44] J. Yoo, M. Yamada, H. Ji, J. Jara-Almonte, and C. E. Myers, *Phys. Plasmas* **21**, 055706 (2014).
- [45] A. Le, W. Daughton, L.-J. Chen, and J. Egedal, *Geophys. Res. Lett.* **44**, 2096 (2017).
- [46] R. Davidson, N. Gladd, C. Wu, and J. Huba, *Phys. Fluids* **20**, 301 (1977).
- [47] Y. Ren, L. Dai, C. Wang, and B. Lavraud, *J. Geophys. Res.* **128**, e2022JA031242 (2023).
- [48] M. Yamada, H. Ji, S. Hsu, T. Carter, R. Kulsrud, N. Bretz, F. Jobes, Y. Ono, and F. Perkins, *Phys. Plasmas* **4**, 1936 (1997).
- [49] J. Yoo, Y. Hu, J.-Y. Ji, H. Ji, M. Yamada, A. Goodman, K. Bergstedt, W. Fox, and A. Alt, *Phys. Plasmas* **29**, 022109 (2022).
- [50] J. Yoo, B. Na, J. Jara-Almonte, M. Yamada, H. Ji, V. Roytershteyn, M. R. Argall, W. Fox, and L.-J. Chen, *J. Geophys. Res.* **122**, 9264 (2017).
- [51] H. Ji and W. Daughton, *Phys. Plasmas* **18**, 111207 (2011).
- [52] S.-L. Chen and T. Sekiguchi, *J. Appl. Phys.* **36**, 2363 (1965).
- [53] J. Ng, J. Yoo, L.-J. Chen, N. Bessho, and H. Ji, *Phys. Plasmas* **30**, 042101 (2023).
- [54] H. Tanabe *et al.* (The MAST Team), *Phys. Rev. Lett.* **115**, 215004 (2015).
- [55] I. H. Cairns and B. F. McMillan, *Phys. Plasmas* **12**, 102110 (2005).
- [56] See Supplemental Material at <http://link.aps.org/supplemental/10.1103/PhysRevLett.132.145101> for physics of anomalous resistivity of lower hybrid drift waves.
- [57] Jongsoo Yoo, Version 1, Name of Repository—Princeton Data Commons (2024), 10.34770/5dj3-jz14.